A Home-Based Bilateral Rehabilitation System With sEMG-based Real-Time Variable Stiffness

Yi Liu, *Student Member, IEEE*, Shuxiang Guo, *Senior Member, IEEE*, Ziyi Yang, Hideyuki Hirata, and Takashi Tamiya

***Abstract*—Bilateral rehabilitation allows patients with hemiparesis to exploit the cooperative capabilities of both arms to promote the recovery process. Although various approaches have been proposed to facilitate synchronized robot-assisted bilateral movements, few studies have focused on addressing the varying joint stiffness resulting from dynamic motions. This paper presents a novel bilateral rehabilitation system that implements a surface electromyography (sEMG)-based stiffness control to achieve real-time stiffness adjustment based on the user's dynamic motion. An sEMG-driven musculoskeletal model that incorporates the muscle activation and muscular contraction dynamics is developed to provide reference signals for the robot's real-time stiffness control. Preliminary experiments were conducted to evaluate the system performance in tracking accuracy and comfortability, which showed the proposed rehabilitation system with sEMG-based real-time stiffness variation achieved fast adaption to the patient's dynamic movement as well as improving the comfort in robot-assisted bilateral training.**

***Index Terms*—Bilateral rehabilitation, exoskeleton, real-time stiffness control, surface electromyography (sEMG).**

I. Introduction

ALONG with the globally growing life expectancy, the incidence of age-related diseases including stroke is increasing rapidly [1]. Acute stroke is the beginning of a long-term struggle with physical damage and the subsequent disability. It is reported that 15% of stroke survivors need long-term health care, while over 70% are left with a significant functional impairment in performing the activities of daily living (ADLs) [2]. This situation creates a massive demand for stroke rehabilitation. However, conventional rehabilitation therapy still remains focused on the in-hospital phase, with its emphasis on intensive manual therapy by the physical therapist, which is a labor-intensive process and consumes significant medical resources. In order to reduce the therapists' burden as well as delivering meaningful restorative therapy to stroke patients, robot-assisted rehabilitation technology has been deployed in the recovery process [3]. Compared to conventional manual therapy, robot-assisted therapy has the potential to offer intensive and repetitive rehabilitation practices with less therapist assistance. Additionally, the embedded sensors in robots augment the therapist's toolbox and facilitate a quantitative evaluation of the patient's recovery [4]. Relevant studies have shown positive outcomes of robot- assisted therapy on improving the motor function of stroke patients [5]–[7].

As one of the common functional disabilities for stroke survivors, hemiparesis is a slight paralysis on one side of the body. Evidence suggests that simultaneous bimanual movements can help patients with hemiparesis to improve the control ability of the affected limb [8]. Accordingly, robot-assisted bilateral rehabilitation involving both arms has been proposed in order to improve rehabilitation efficiency and facilitate individual's recovery [9]. Different from unilateral arm rehabilitation merely aimed at the affected side [10], [11], bilateral arm rehabilitation emphasizes on a superior level of motor coordination by exploiting the patient's contralateral side to generate synchronized movements on the affected side [12]. However, it remains a significant challenge for robotic systems to explore human-like properties during robot-assisted training.

In biology, joint stiffness is assumed as an essential physical property to describe human dynamic movements. Several biomechanical studies indicate that the human joint stiffness varies considerably during movement [13], [14]. As a result, dynamic control of joint stiffness is a crucial factor in enabling rehabilitation robots to explore human-like behavior patterns and ensure comfortable coordinated movements.

Although various research has made progress in promoting synchronized robot-assisted bilateral movement [15], [16], few studies have focused on addressing the varying joint stiffness resulting from dynamic motions. Given that the human movement is caused by the co-contraction of the antagonistic muscle pairs

Manuscript received November 15, 2019; revised March 21, 2020, June 17, 2020, and August 9, 2020; accepted September 22, 2020. Date of publication September 29, 2020; date of current version May 11, 2021. This work was supported in part by National High Tech. Research and Development Program of China under Grant 2015AA043202, and in part by SPS KAKENHI under Grant 15K2120 *(Corresponding author: Shuxiang Guo.)*

Yi Liu and Ziyi Yang are with the Graduate School of Engineering, Kagawa University, Takamatsu 761-0396, Japan (e-mail: s18d504@stu.kagawa-u.ac.jp; s19g533@stu.kagawa-u.ac.jp).

Shuxiang Guo is with the Key Laboratory of Convergence Medical Engineering System and Healthcare Technology, the Ministry of Industry and Information Technology, Beijing Institute of Technology, Beijing 100081, China, and also with the Department of Intelligent Mechanical Systems Engineering, Kagawa University, Takamatsu 761-0396, Japan (e-mail: guo@eng.kagawa-u.ac.jp).

Hideyuki Hirata is with the Department of Intelligent Mechanical Systems Engineering, Kagawa University, Takamatsu 761-0396, Japan (e-mail: hhirata@eng.kagawa-u.ac.jp).

Takashi Tamiya is with the Department of Neurological Surgery, Faculty of Medicine, Kagawa University, Takamatsu 761-0793, Japan (e-mail: tamiya@med.kagawa-u.ac.jp).

Digital Object Identifier 10.1109/JBHI.2020.3027303

2168-2194 © 2020 IEEE. Personal use is permitted, but republication/redistribution requires IEEE permission.
See https://www.ieee.org/publications/rights/index.html for more information.

Authorized licensed use limited to: Tianjin University of Technology. Downloaded on May 13,2021 at 11:53:56 UTC from IEEE Xplore. Restrictions apply.

acting on the joint, joint stiffness is assumed as an outcome of the muscle activity [17]. Namely, the muscle activation has access to measure real-time joint stiffness. Surface electromyography (sEMG) was presented as a non-invasive measurement method to describe muscle activation dynamics [18]. As a biological signal generated by muscle contraction, the sEMG signal has broad applications in pattern classification [19], [20] and intention-based myoelectric control [21], [22]. Notably, recent studies indicate that sEMG signals captured on the contralateral side may provide meaningful guidance to regulate the robotic assistance for the affected arm [23].

In this paper, we present a novel bilateral rehabilitation system that implements an sEMG-based stiffness control to achieve real-time stiffness adjustment of the exoskeleton device. The proposed system can capture the user's real-time motions on the contralateral side and generate a motion-related stiffness variation to adapt to the user's dynamic motions. To the best of our knowledge, this is the first work focused on the real-time stiffness adjustment based on the sEMG signals from the patient's contralateral side for upper limb bilateral rehabilitation.

The rest of this paper is organized as follows: in Section II, we first introduce the hardware platform and the control strategy of the proposed bilateral rehabilitation system. In Section III, an sEMG-driven musculoskeletal model is presented, following by validation processes in both isometric and dynamic contractions. Then, we introduce the preparation of online joint stiffness control in Section IV. The experiments for characterizing the performance of the proposed bilateral system are conducted in Section V and discussed in Section VI. Finally, the conclusions are drawn in Section VII.

II. Methods

In the proposed home-based bilateral rehabilitation system, a powered variable-stiffness exoskeleton device (PVSED) is utilized as the hardware platform to implement an sEMG-based real-time joint stiffness control for robot-assisted bilateral training.

A. Hardware Platform

1) Overview of the PVSED: The design of the PVSED was introduced in detail in our previous research [24]. It is a powered elbow rehabilitation device characterized by the features of high portability and light weight. In order to facilitate home-based rehabilitation setups, the PVSED is designed to be carried on a wearer's back via shoulder straps and belts, as shown in Fig. 1. For reducing the structural weight as well as cost, the main exoskeletal frames were manufactured by light-weight aluminum alloys and several connection parts were fabricated by 3D printing using ABS plastic. The total weight of the PVSED is only 3.1 kg and shared by two shoulder straps and a belt attached to the torso, which has minimal effects on the wearer's body.

Since the position of the center of the glenohumeral joint is changed during the upper limb movements [25], 3 passive shoulder degrees of freedom (DoFs) including shoulder adduction/abduction, shoulder flexion/extension and internal/external rotation of upper limb are designed for the proposed PVSED to minimize the misalignment of the exoskeletal and the human joint axes as well as making allowance for the user's natural range of motion. Additionally, the shoulder breadth and shoulder-elbow length of the PVSED can be configured based on each individual's body size due to the adjustable design of the back frame and upper limb frame. The resulting high portability and compatibility not only facilitate home-based rehabilitation setups but also broaden its usage scenarios in daily life. The specification of the PVSED is reported in Table I.

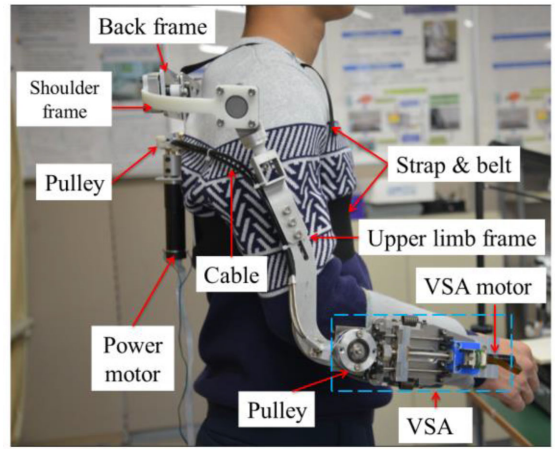

Fig. 1. Physical prototype of the PVSED.

TABLE I
SPECIFICATION OF THE PVSED

	Motion	Range
Shoulder joint (Passive DoFs)	abduction/adduction	[0°, 90°]
	flexion/extension	[-45°, 125°]
	Internal/external rotation	[-80°, 70°]
Elbow joint (Active DoF)	flexion/extension	[0°, 135°]
Back frame	Shoulder breadth adjustment	300-450 mm
Upper limb frame	shoulder-elbow length adjustment	250-380 mm

※Passive DoFs: Passive rotation caused by human motions; Active DoF: Active rotation controlled by the cable-driven mechanism.

As a powered rehabilitation device, the PVSED can assist the wearer's elbow motion via a light-weight cable-driven mechanism. A compact DC motor (Maxon RE-30 Graphite Brushes Motor) fixed to the back panel is used to transmit the power by a steel cable threaded through a pulley at the elbow joint. In order to adapt to the individual's impairment level of the upper limb, the stiffness of the exoskeleton device is designed to be adjustable, with the aid of an integrated variable stiffness actuator (VSA). The VSA is integrated into the forearm part, equipped with a small-size DC motor (Maxon RE-13 Graphite Brushes Motor) to regulate the joint stiffness of the PVSED. For a clear overview, the detailed structure of the integrated VSA is shown in Fig. 2. A pivot, independently actuated by the Maxon RE-13 motor through ball screw transmission, is movable along with a slot in the lever. The slot-side end of the

Authorized licensed use limited to: Tianjin University of Technology. Downloaded on May 13,2021 at 11:53:56 UTC from IEEE Xplore. Restrictions apply.

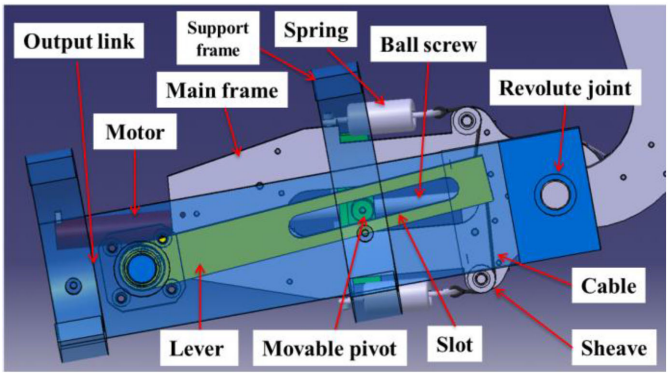

Fig. 2. Structure of the integrated VSA.

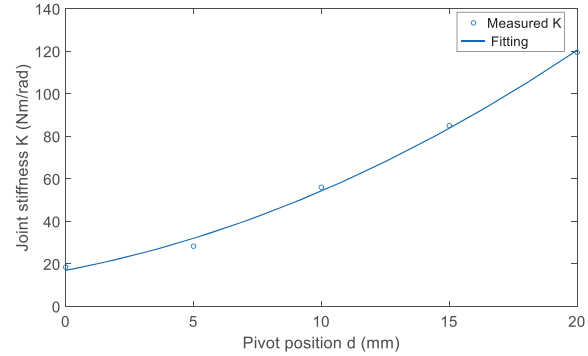

Fig. 4. Pivot-to-stiffness curve.

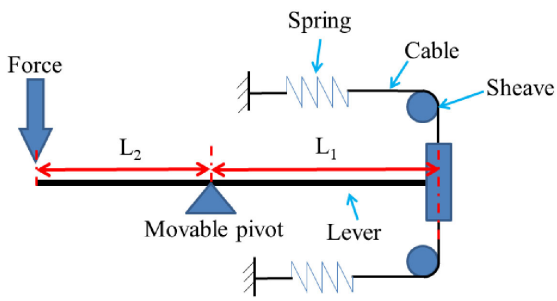

Fig. 3. Schematic of the VSA. The stiffness variation is achieved by a movable pivot to change the transmission ratio of the lever arm.

lever is connected to a pair of antagonistic springs fixed to the main frame, while the opposite end is connected to the output link worn by the user. The output link and the cable-driven main frame are linked through a revolving shaft at the elbow joint. Due to the preload force generated by the springs, they can rotate conjointly to perform synchronized elbow flexion and extension without angular displacement. However, once the external force acting on the output link exceeds spring preload, one of the antagonistic springs will be elongated, thus causing a deflection between the main frame and the output link [24]. This resulting "passive compliance" can restrain an excessive interaction force due to undesired human motions (i.e., spasms, etc.), which is an essential factor for rehabilitation robots to minimize the potential risk to patients. Furthermore, the level of passive compliance can be adjusted by regulating the transmission ratio between the internal elastic elements and the output link.

The schematic of stiffness adjustment is shown in Fig. 3. A force acting on the output link is balanced by the spring force, i.e., $F \cdot L_2 = F_{spring} \cdot L_1$. Following the definition of stiffness, the output stiffness K is represented by

$$K = \frac{F \cdot l}{\theta_d} = \frac{F_{spring} \cdot l}{\theta_d} \cdot \frac{L_1}{L_2} \tag{1}$$

where F_{spring} is the spring force, l is the moment arm which is a constant value, θ_d is the output deflection, and L_1/L_2 is the transmission ratio.

It is observed that the stiffness K depends on the transmission ratio L_1/L_2. Thus, by moving the pivot position to change the transmission ratio, the output joint stiffness can be adjusted. Compared to the active stiffness adjustment achieved by closed-loop impedance control [26], applying the VSA to regulate the robot stiffness is more reliable and safer, since the stiffness provided by the VSA is an inherent characteristic only related to the pivot position, without requiring any extra closed-loop control.

2) Pivot-to-Stiffness Identification: In order to explore the relationship between the pivot position and the resulting stiffness of the VSA, a force-deflection trial was carried out in five different pivot positions (from 0 mm to 20 mm with an increment of 5 mm). Note that 0 mm is defined as the starting position of the slot in the lever arm towards the antagonistic springs. In the trial, a force was exerted to rotate the elbow joint, whereas the output link was blocked by a force sensor (MINI 4/20, BL AUTOTEC. Ltd.). As a result, the deflection between the elbow joint and the output link was generated and recorded by an angle sensor (MTx sensor, Xsens Technologies B.V., the Netherlands). By substituting the moment arm of 215 mm, the stiffness in each pivot position was calculated according to Eq. (1) and plotted in Fig. 4. Furthermore, a 2nd-order polynomial fitting based on least-squares approximation was applied to describe the pivot-stiffness relationship, which is expressed by

$$\mathrm{K} = 0.1443d^2 + 2.287d + 16.95 \ \ (0 \leq d \leq 20 \text{ mm}) \tag{2}$$

Therefore, by moving the pivot position d, the stiffness of the VSA can be adjusted to a desired level to adapt to the individual's physical condition and the rehabilitation training intensity.

B. sEMG-based Joint Stiffness Control for Bilateral Training

Bilateral rehabilitation training involves the participation of both arms to complete collaborative tasks. During bilateral exercise, the affected side is desired to follow the movement pattern of the contralateral side with the aid of the rehabilitation robot. In order to achieve natural and comfortable coordinated movements, the rehabilitation robot should not only track the patient's elbow trajectory but also adapt to the varying joint stiffness due to dynamic motions. Since the stiffness profiles of the elbow joint vary with respect to the upper limb position

Authorized licensed use limited to: Tianjin University of Technology. Downloaded on May 13,2021 at 11:53:56 UTC from IEEE Xplore. Restrictions apply.

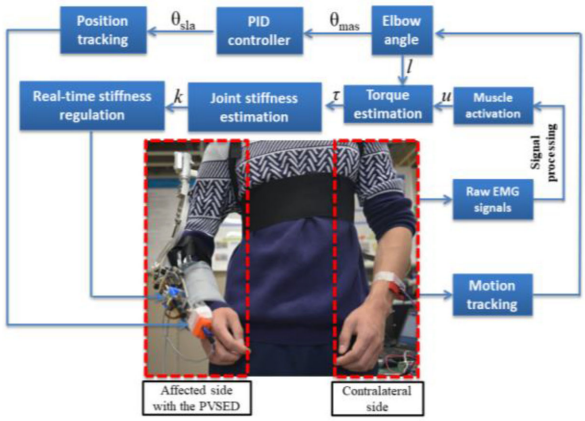

Fig. 5. Proposed bilateral training strategy using sEMG-based stiffness control.

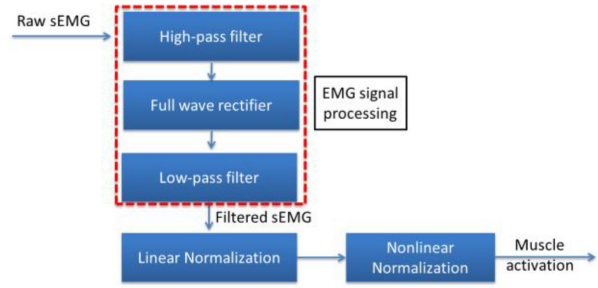

Fig. 6. Flow chart of the EMG processing procedure.

and the co-contraction of antagonistic muscles [27], we propose an sEMG-based real-time joint stiffness control that makes use of the sEMG signals and elbow angle on the contralateral side as input to dynamically adjust the stiffness of the exoskeleton device during bilateral movement. The diagram of the proposed method is shown in Fig. 5. An inertial measurement unit (GY-25 tilt angle module) is attached to the subject's contralateral side to track his/her voluntary elbow movements. The sampled elbow angle θ_{mas} is sent to the PID controller for master-slave position tracking. Meanwhile, the raw sEMG signals on the same side are collected by dry electrodes and subsequently processed to obtain the real-time muscle activation u of the biceps brachii (BB) and the triceps brachii (TB) respectively. Based on the musculoskeletal geometry of the upper limb, the muscle-tendon length l can be calculated according to the measured elbow angle. Once the muscle activation u and muscle-tendon length l are known, the corresponding muscle force and torque can be estimated using the musculoskeletal model presented in Section III. Furthermore, the elbow joint stiffness is deduced from the antagonistic muscle torques and used as reference signals to guide the stiffness regulation of the VSA. By means of real-time stiffness adjustment, the proposed rehabilitation system has the potential to adapt to the patient's dynamic motion and provide appropriate power assistance.

III. sEMG-driven Musculoskeletal Model

In this section, an sEMG-driven musculoskeletal model is developed to characterize the physical properties of the elbow joint, in which not only the muscle activation but also the muscular contraction dynamics are taken into consideration.

A. Measurement of Muscle Activation

EMG signals generated by the neural impulses to activate the muscle fibers can be used to measure the muscle activation dynamics. In our study, the EMG signals are collected by a commercial EMG device (Personal-EMG, Oisaka Electronic Equipment Ltd., JAPAN). The sampling rate is 1000 Hz, with a differential amplification of 1000 and a common-mode rejection of 104 dB. In order to measure the real-time muscle activation, the raw signals need to be processed by following the procedure shown in Fig. 6. Firstly, the sampled signals are filtered by an accessory high-pass filter box with a cut-off frequency of 10 Hz to remove DC offsets and the noises in the low-frequency range. Then, a full wave rectifier is used to acquire the absolute value of the EMG signals. Thirdly, a digital filter (1st-order, low-pass Butterworth filter with a cut-off frequency of 2 Hz) is applied to extract the envelope of the EMG signals [28]. Considering the amplitude of EMG signals are strongly influenced by the given detection condition, e.g., electrode sites, inter-subject variability, etc., normalization methods are needed to overcome this uncertainty [29]. After the signal pre-processing, the filtered signals EMGα is linearly normalized to a value between 0 and 1 by dividing its peak value $\mathrm{EMG_{MVC}}$ obtained from the maximum voluntary contraction (MVC) test, i.e., u=EMGα/ $\mathrm{EMG_{MVC}}$. Finally, the normalized signals are transformed to the muscle activation level by applying the following nonlinear normalization [30]:

$$a\left(u\right) = \frac{e^{Au} - 1}{e^{A} - 1} \tag{3}$$

where u denotes the processed sEMG signals, and A is a nonlinear shape factor between 0 and -3.

B. Muscle Contraction Dynamics

Stimulated by nerve impulses, a muscle would generate a neural-stimulation active tension, a tissue-related passive tension and the accompanying unavoidable perturbations caused by the active and passive tension, while the tendon in series with the muscle is used to transmit the total tension [31]. Referencing the working principle of muscle units, a Hill-type muscle model was proposed to describe the muscle properties [32]. A conventional Hill-type muscle model consists of an active contractile element (CE), a passive parallel elastic element (PE) and a series elastic element (SE). Elbow flexion and extension in the sagittal plane are principally accomplished by the concentric/eccentric contraction of an antagonistic muscle pair (BB and TB). In our study, we established a musculoskeletal model to describe the muscle contraction dynamics during human elbow movements. In the proposed model, the upper limb is represented by a pair of

Authorized licensed use limited to: Tianjin University of Technology. Downloaded on May 13,2021 at 11:53:56 UTC from IEEE Xplore. Restrictions apply.

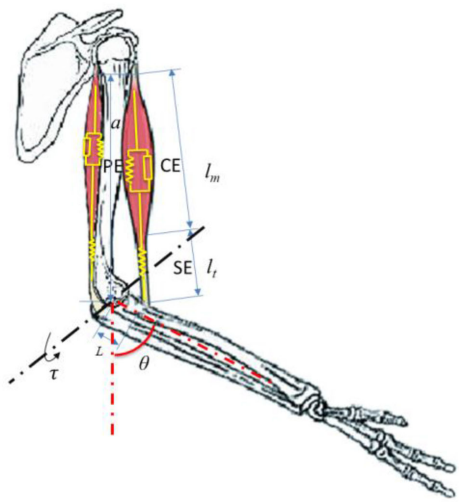

Fig. 7. Musculoskeletal model of the upper limb. The biceps brachii and triceps brachii are a pair of antagonistic muscles for elbow flexion/extension in the sagittal plane. Each muscle is modeled as an active contractile element (CE) in parallel with a passive elastic element (PE), while the tendon is modeled as a series elastic element (SE). θ is the elbow angle from the initial position oriented perpendicular to the ground.

antagonistic muscle-tendon units with bones for simplification. As shown in Fig. 7, the muscle-tendon units of BB and TB are respectively described by the Hill-type muscle model, while the bones are regarded as the rigid elements.

Since the muscle and tendon act like springs in series [33], the muscle-tendon force can be represented by

$$F^{mt} = F^t = F^m \cdot cos\varphi \tag{4}$$

where φ is the pennation angle.

A small pennation angle may have limited effects on estimating the muscle force [34]. According to biomechanical literature [35], the pennation angle of BB is nearly 0° and that of TB is smaller than 10°. Therefore, the effect of the pennation angle is ignored, i.e., $F^{mt}=F^m$.

Since the muscle fiber can be represented by a CE in parallel with a PE, the muscle force is described by

$$F^m = F_{CE} + F_{PE} \tag{5}$$

The CE is assumed to produce an active contractile force and the PE is assumed to produce a passive elastic force, which can be calculated by Eq. (6) and ((7)), respectively.

$$F_{CE} = F_{max} \cdot f_L(l) \cdot f_V(v) \cdot a(u) \tag{6}$$

$$F_{PE} = F_{max} \cdot f_P(l) \tag{7}$$

where F_{max} is the maximum isometric muscle force, $a(u)$ is the muscle activation obtained by Eq. (3). $f_L(l)$ and $f_V(v)$ represent the normalized active force-length and force-velocity relationship respectively, and $f_P(l)$ denotes the normalized passive force-length relationship.

To simplify biomechanical parameters in the calculation, a 2nd-order polynomial fitting is applied to obtain $f_L(l)$ [36], which is expressed by

$$f_L(l) = \begin{cases} q_0 + q_1 \cdot l + q_2 \cdot l^2, & 0.5 \le l \le 1.5 \\ 0, & \text{otherwise} \end{cases} \tag{8}$$

where q_0=-2.06, q_1=6.16, and q_2=-3.13 are set as constants. $l = l^m/l_o^m$ is the normalized muscle length, and l_o^m denotes the optimal muscle fiber length.

The normalized force-velocity relationship $f_v(v)$ is given by

$$f_V(v) = \frac{0.1433}{\left(0.1074 + e^{-1.3\sinh(2.8v+1.64)}\right)} \tag{9}$$

where $v = v_m/v_{max}$, v_m is the muscle contraction velocity which is the derivative of the muscle fiber length l_m. It is reported that the maximum muscle contraction velocity v_{max} is nearly equal to $10l_o^m/s$ [37], which far exceeds v_m. As a result, $f_V(v)$ can be set to 1 for simplification.

The $f_P(l)$ in Eq. (7) was derived from a normalized passive force-length curve [38], which is calculated by

$$f_p(l) = e^{10 \cdot l - 15} \tag{10}$$

In order to decrease the calculation complexity, the parameters F_{max}, φ and l_m^o are assumed to be constants [39]. Deduced from Eq. (5) - *(10)*, the muscle force F^m is expressed as a function of the real-time muscle activation level $a(u)$ and muscle fiber length l^m.

The muscle-tendon length consists of the muscle fiber length and the tendon length, i.e.,

$$l^{mt} = l^m \cdot cos\varphi + l^t \tag{11}$$

where l^m represents the muscle fiber length, l^t represents the total length of the tendon, and φ is the negligible pennation angle as stated above.

Given that the tendon is relatively stiff, its length can be regarded as a constant during movement. Therefore, once the muscle-tendon length in the current position is known, the corresponding muscle fiber length l^m can be calculated.

Based on the musculoskeletal geometry shown in Fig. 7, the muscle-tendon length of the biceps brachii acting on the elbow joint can be obtained by

$$l_{BB}^{mt} = \sqrt{a^2 + L^2 - 2aLcos(\pi - \theta)} \tag{12}$$

where a is the length of the upper arm, L is the distance from the axis of the elbow joint to the bone-tendon junction in the forearm, and θ is the elbow angle.

Considering the bone-tendon junction of the triceps brachii is much near the elbow joint, the muscle-tendon length of the triceps brachii can be simplified by a 1st-order polynomial of the elbow angle θ [36]:

$$l_{TB}^{mt} = b_0 + b_1\theta \tag{13}$$

where b_0 and b_1 are constants.

Based on the displacement method in [40], the moment arm of a muscle-tendon unit can be obtained by

$$r = \frac{\partial l^{mt}(\theta)}{\partial \theta} \tag{14}$$

Authorized licensed use limited to: Tianjin University of Technology. Downloaded on May 13,2021 at 11:53:56 UTC from IEEE Xplore. Restrictions apply.

Thus, the torque contributed by a single muscle-tendon unit is given by

$$\tau = F^{mt} \cdot r \tag{15}$$

Since elbow flexion and extension are principally performed by a pair of antagonistic muscles (BB and TB), the net torque acting on the elbow joint is

$$\tau_{elbow} = |\tau_{BB}| - |\tau_{TB}| = \left|F^{mt}_{BB} \cdot r_{BB}\right| - \left|F^{mt}_{TB} \cdot r_{TB}\right| \tag{16}$$

It is reported that the joint stiffness increases with the amount of the antagonistic muscle torques [41]. Therefore, the stiffness trend index (STI) is defined as

$$STI = |\tau_{BB}| + |\tau_{TB}| \tag{17}$$

The STI is linearly mapped to the robot stiffness K, which is written as

$$K = \alpha \cdot STI + \beta \tag{18}$$

where α (rad^{-1}) and β (Nm/rad) are constants depending on the task requirements and individual physical condition. For a patient with an altered intrinsic joint stiffness due to spasticity, the robot stiffness may be set to an appropriate range by adjusting the proportional parameter α.

C. Model Identification and Validation

For the reason that some physiological parameters (e.g., the optimal fiber length l^o_m, tendon length l_t, the tendon-to-elbow distance L) described in the musculoskeletal model cannot be measured directly, their initial values were set according to the literature [35]. In order to minimize the uncertainty of the musculoskeletal model, those parameters need to be identified based on each individual's experimental data. In our study, the experiments were conducted in isometric and dynamic muscle contraction respectively. This study was approved by the Institutional Review Board (IRB) in the Faculty of Engineering, Kagawa University (*Ref. No. 01-011*). Ten healthy subjects (males, average age: 25.6 ± 3.7 years old; average weight: 69.4 ± 10.2 kg; average height: 178.1 ± 7.1 cm) were enrolled in this study after signing a written consent.

1) Isometric Contraction: In isometric contraction, the muscle is activated to contract but does not shorten or extend [42]. Consequently, the muscle-tendon length is regarded as constant. The experimental setup for isometric contraction is shown in Fig. 8. The subject's forearm was held in the horizontal position with a fixed elbow angle of 90°. In this posture, the participation of TB may be ignored [43]. Before attaching the electrode to the muscle belly, the subject's skin surface was cleaned by alcohol to decrease its impedance. A bipolar surface electrode (Oisaka Electronic Equipment Ltd., Japan) was attached to BB and aligned parallel to the muscle fibers on the subject's left arm to sample the sEMG signals. Moreover, a 6-axis force sensor (MINI 4/20, BL AUTOTEC. Ltd., Japan) was fastened to a fixed bracket. In the experiment, the subjects were instructed to exert a gradually increasing force on the fastened force sensor to his/her maximum and then return to relaxed state. Throughout the process, subjects maintained their forearms horizontally without elbow rotation and used their fingertips to push the force sensor along Y axis. The sEMG and force signals were simultaneously acquired by the above sensors. The sampled sEMG signals were subsequently processed to estimate the muscle force F^{mt}.

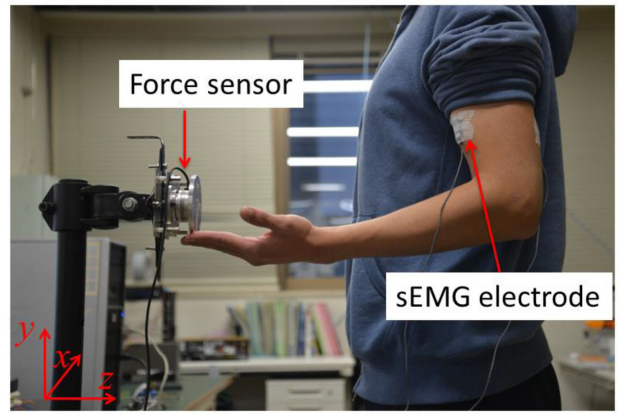

Fig. 8. Experimental setup of the model identification in isometric contraction.

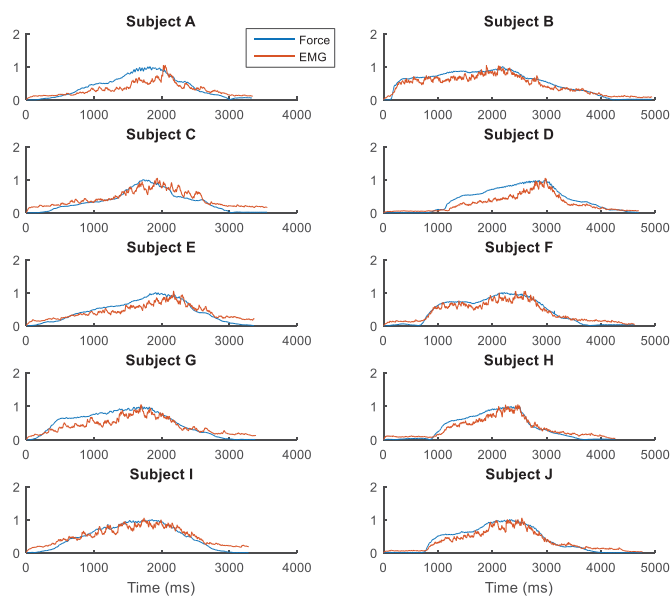

Fig. 9. Real-time force estimation using sEMG signals. The red curve represents the predicted force estimated by the subject's muscle activation, while the blue curve represents the measured force signals recorded by the 6-axis force sensor.

This trial was repeated ten times for each subject. A 3-minute interval was set between every two trials in order to avoid muscular fatigue. The first five trials were chosen to identify the individual's musculoskeletal parameters, while the remaining trials were used for model validation. Fig. 9 shows one set of the validation trial of the ten subjects, where the red curve represents the estimated force using the Hill-type muscle model, while the blue curve represents the measured force recorded by the force sensor. In order to decrease the possible contamination due to other joints or muscle participation, the measured force signal was also normalized to a percentage value of its peak amplitude.

Authorized licensed use limited to: Tianjin University of Technology. Downloaded on May 13,2021 at 11:53:56 UTC from IEEE Xplore. Restrictions apply.

TABLE II
CORRELATION COEFFICIENT BETWEEN THE sEMG-BASED PREDICTED FORCE AND THE MEASURED FORCE (p<0.01)

Subject	A	B	C	D	E	F	G	H	I	J
R^2	86.7%	96.9%	93.2%	89.3%	92.2%	97.7%	90.4%	96.3%	96.5%	97.0%

It can be seen that the envelope of the model-predicted force reflected a high correlation with that of the measured force. The average correlation coefficient (p<0.01) of all validation trials for each subject are reported in Table II. It is observed that the correlation coefficient for Subject A is 86.7%, while that for Subject F is 97.7%. This difference partly resulted from the inter-subject variability of sEMG signals. Also, the simplified physiological parameters in the established musculoskeletal model may have effects on this. Overall, the results among all subjects showed that the proposed musculoskeletal model has a satisfying performance for real-time muscle force estimation in isometric contraction.

2) Dynamic Contraction: In dynamic muscle contractions including concentric and eccentric contraction, the muscle contracts and shortens/extends, which leads to a varying muscle-tendon length. To further evaluate the performance of the proposed musculoskeletal model for dynamic contractions, one healthy subject (Male, Height: 175 cm, Weight: 75 kg) participated in a trial to perform continuous elbow flexion/extension in the sagittal plane. An MTx angle sensor is attached to the subject's upper limb to record the elbow angle θ. Meanwhile, the raw sEMG signals from BB and TB were sampled by a pair of dry electrodes and subsequently processed to obtain the muscle activation *a(u)*. The muscle activation *a(u)* and elbow angle θ were substituted to the musculoskeletal model to estimate the real-time joint torque by following the procedures described in Section III. B.

The reference torque applied to the subject's elbow joint can be deduced from a kinematic and dynamic model of the upper limb [44], which is presented by

$$\tau = I \cdot \ddot{\theta}_e + \tau_g \tag{19}$$

where I is the inertia moment of the forearm, $\ddot{\theta}_e$ is the angular acceleration of the elbow joint, and τ_g is the gravitational torque caused by the mass of the forearm.

Given that the elbow movement in rehabilitation is allowed to perform with a relatively low angular velocity, the resulting angular acceleration is negligible. Thus, the joint torque τ can be represented by

$$\tau = \tau_g = m_f \cdot g \cdot l_f \cdot \sin\theta_e \tag{20}$$

where m_f is the total mass of the forearm, l_f is the length from the center of mass of the forearm to the elbow joint, and θ_e is the elbow angle.

The m_f and l_f may be estimated based on the individual's physical parameters [45], which are written as

$$m_f = m \cdot 0.6\% + m \cdot 1.9\% \tag{21}$$

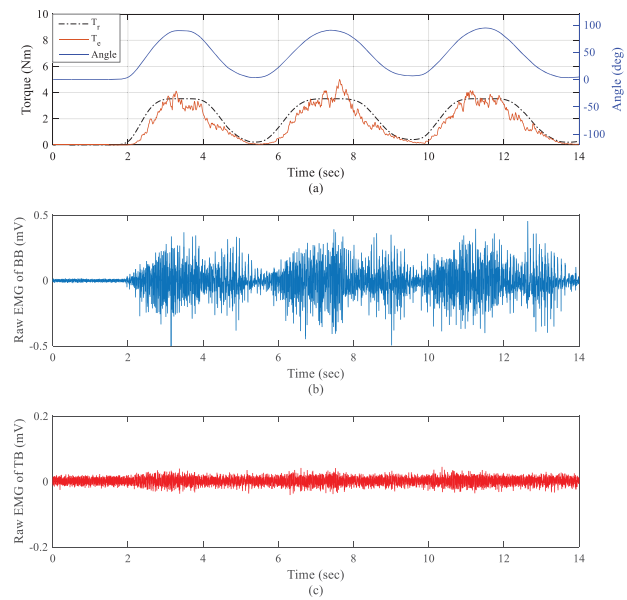

Fig. 10. Dynamic validation of the sEMG-driven musculoskeletal model. (a) τ_r is the reference torque deduced from the kinematic and dynamic model, while τ_e is the estimated torque obtained by the sEMG-driven musculoskeletal model. (b) Raw sEMG signals of BB. (c) Raw sEMG signals of TB.

$$l_f = \frac{m \cdot 0.6\% \cdot \left(\frac{10.4\% H}{2} + 15.7\% \cdot H\right) + m \cdot 1.9\% \cdot 15.7\% \cdot \frac{H}{2}}{m \cdot 0.6\% + m \cdot 1.9\%} \tag{22}$$

where m and H are the individual's weight and height, respectively. Substituting the subject's physical parameters (75 kg/1.75 m) to the formula above, we can obtain the m_f and l_f (1.875 kg/ 0.1922 m).

In the experiment, the subject was instructed to perform continuous elbow flexion-extension ten times. Fig. 10(a) shows a segment of the experimental results, including the estimated joint torque τ_e predicted by the sEMG-driven musculoskeletal model and the reference joint torque τ_r deduced from the kinematic and dynamic model, along with the trajectory of the elbow joint. Additionally, the raw sEMG signals of BB and TB are shown in (b) and (c), respectively.

For evaluating the proposed sEMG-driven musculoskeletal model, the root mean square error (RMSE) between the reference torque τ_r and the estimated torque τ_e was calculated as follows:

$$RMSE = \sqrt{\frac{\sum_{i=1}^{n} \left(\tau_r(i) - \tau_e(i)\right)^2}{n}} \tag{23}$$

Authorized licensed use limited to: Tianjin University of Technology. Downloaded on May 13,2021 at 11:53:56 UTC from IEEE Xplore. Restrictions apply.

The average RMSE for all trials was 0.6408 Nm. Furthermore, the normalized root mean square error (NRMSE) was obtained by

$$NRMSE = \frac{RMSE}{\tau_{e_max} - \tau_{e_min}} \tag{24}$$

where τ_{e_max} and τ_{e_min} are the maximum and minimum estimated torque, respectively.

The NRMSE is equal to 12.52%. Considering the effects of the inherent instability of sEMG signals and the neglected factors (e.g., the moment of inertia) in deducing the reference torque, this error is still acceptable.

IV. Preparation of Online Stiffness Control

By the offline experimental analysis in the previous section, the proposed sEMG-driven musculoskeletal model was validated in both isometric and dynamic muscle contractions. However, in order to be used in online joint stiffness control, there are still some issues that need to be addressed. Firstly, the sEMG signals are intrinsically non-stationary, which may result in unavoidable steep amplitude spikes [29]. Although these spikes do not affect the model identification in the offline experiment, they may affect the robustness of the robot control. Secondly, similar to other biological signals (e.g., EEG [46], ECG [47], etc.), it is difficult or even impossible to reproduce the identical signal shape for the same motion [48]. Instead, we can extract the features of sEMG signals to characterize the signal development for a specific motion. The signal features can be extracted in time domain, frequency domain and time-frequency domain [49]. Based on the square root calculation in the time-domain window, root mean square (RMS) can outline the mean trend of the signals and cut away the signal spikes.

$$RMS = \sqrt{\frac{1}{N}\sum\nolimits_{i=1}^{N} \alpha_i^2} \tag{25}$$

where N is the number of data points, and α_i is the filtered sEMG signals after the signal pre-processing. In this study, a nonoverlapping sliding window containing 20 data points (N=20) was chosen in order to achieve a fair trade-off between the control robustness and fidelity. The calculated RMS is subsequently rectified by the successive linear and nonlinear normalization to obtain the muscle activation as stated before.

V. Experiment and Characteristic Evaluation

A. Characterization of the sEMG-based Real-time Variable Stiffness

In order to facilitate an effective rehabilitation process, the robotic systems should exploit the patient's physical capabilities and offer proper stiffness range to provide assistance as needed in different training intensities. When the patient performs rehabilitation training with no load, the robot stiffness is desired to be adjusted in real time to adapt to the varying reflex stiffness of the human limb. With the gradual increase of training intensity, the robot should allow the patient to intentionally increase the robot stiffness so as to obtain sufficient assistance. For evaluating the feasibility of the proposed sEMG-based real-time stiffness control method, a weight lifting task was designed and performed by ten subjects. In the trial, the subjects were instructed to lift a dumbbell in the sagittal plane with different weights (0 kg, 1 kg, and 2 kg), which simulates different intensities of rehabilitation training. Two dry electrodes were attached to BB and TB to collect the sEMG signals. Fig. 11 shows the RMS of sEMG signals from Subject A, along with the real-time stiffness of the VSA at each level of intensity. As we can see, the stiffness of the VSA continuously varied with respect to the RMS of sEMG signals, by following the relationship described in the musculoskeletal model. Moreover, with the increase of the lifting load, the RMS values were also augmented due to the increased muscle contraction. The stiffness amplitude of the VSA was accordingly enlarged in order to provide enhanced assistance to the user for completing the laborious task. Similar outcomes were observed in other participants. By means of the sEMG-based stiffness control, the robot stiffness can be adjusted in real time based on the subject's physical condition and task requirement. Benefiting from this characteristic, the proposed approach has the potential to provide individual-specific and task-oriented rehabilitation.

B. Performance Evaluation of the Bilateral Rehabilitation System with sEMG-based Real-time Stiffness Variation

To characterize the performance of the proposed bilateral rehabilitation system, a rehabilitation task involving the participation of both arms was designed and conducted on ten subjects. The experimental setups are shown in Fig. 12. A miniature inertial measurement unit (GY-25 tilt angle module) was attached to the subject's left hand to capture the active elbow movements. Meanwhile, the trajectory of the subject's right arm with the PVSED was recorded by an attached MTx angle sensor. In addition, a small-size force sensor (FS03, Honeywell Ltd., U.S.A) was placed into the upper support frame to measure the contact force during elbow movement. In the experiment, the subjects performed voluntary elbow motion on the left side. Meanwhile, the subject's elbow movements on the right side were totally powered by the PVSED to track the elbow movement of the left side. This task simulated a basic bilateral rehabilitation procedure, in which the subject's left arm was regarded as the master side that could move voluntarily, while his right arm equipped with the PVSED was assumed as the slave side to be guided. The functionality of the bilateral rehabilitation system was successively evaluated in tracking accuracy and comfortability.

1) Tracking Accuracy: For comparison, the tracking accuracy of the proposed rehabilitation system was evaluated in four different stiffness settings, including a minimum stiffness of the VSA (pivot position d= 0 mm, K= 18.48 Nm/rad) as low stiffness (LS), a maximum stiffness of the VSA (pivot position d= 20 mm, K= 119.49 Nm/rad) as high stiffness (HS), an average joint stiffness measured in human elbow flexion/extension [50] (pivot position d= 5 mm, K= 28.33 Nm/rad) as medium stiffness (MS), and an sEMG-based variable stiffness (VS).

A segment of the experimental results for Subject A is plotted in Fig. 13. It is seen that a phase offset resulting from the tracking

Authorized licensed use limited to: Tianjin University of Technology. Downloaded on May 13,2021 at 11:53:56 UTC from IEEE Xplore. Restrictions apply.

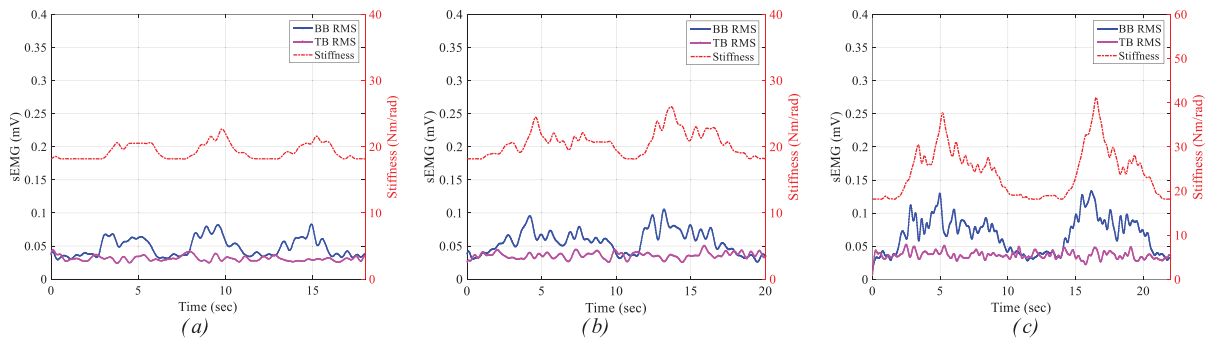

Fig. 11. Real-time stiffness control with different loads. (a) 0 kg. (b) 1 kg. (c) 2 kg. The blue curve represents the RMS value from the biceps brachii, the pink curve represents the RMS value from the triceps brachii, and the red curve is the resulting stiffness of the VSA.

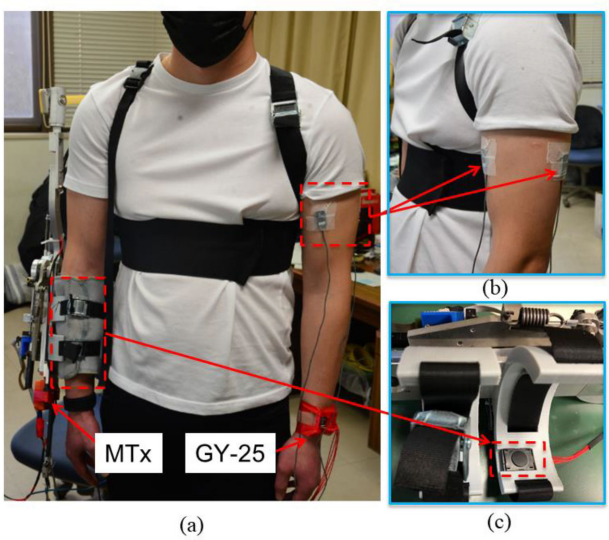

Fig. 12. Experimental setups. (a) Front view of the PVSED with a wearer. (b) Lateral view of the sEMG electrode placements. (c) Detailed view of the FS03 force sensor placement.

error appeared between the master and slave trajectories. In the experiment, the tracking error was principally caused by the gravitational torque from the weight of the forearm, and its range varied due to the stiffness settings. As illustrated in Section II. A, if the load exerted on the output link exceeds the spring preload, the output link will deviate from the cable-driven main frame, thus generating an observed angular deflection. In low stiffness, the PVSED implemented a compliant actuation that makes allowance for relatively larger deviations from the reference position so as to minimize the interaction force. With the increase of the stiffness, the subject's upper limb on the slave side was actuated by a stiffer VSA to achieve more precise position tracking. For the trials with constant stiffness (Fig. 13(a)-(c)), the tracking error increased in the ascending phase while decreased in the descending phase. It is of considerable interest that in the trial with sEMG-based real-time stiffness variation (Fig. 13(d)), the system allowed the slave side to deviate from the reference trajectories, while it attempted to minimize the scale of the deviations throughout the process.

The average tracking error along with standard deviation (SD) of the ten subjects in each stiffness setting is shown in Fig. 14. It is notable that the average tracking error in the VS case was comparable with that in the MS case (4.05° versus 3.63°), although the SD in the former case was more significant (±1.09° versus ±0.47°) owing to the inter-subject variability of sEMG signals.

2) Force Measurement: To further evaluate the comfort of the proposed rehabilitation system, we carried out an experiment to compare the contact force in the MS and VS settings. In the experiment, a bilateral movement task including ten cycles of elbow flexion/extension was completed by ten subjects. For the sake of clarity, only one cycle of elbow motion of Subject A was plotted. Fig. 15(a) and (b) show the measured force along with elbow angle in the MS and VS trials respectively. It needs to be noted that the measured contact force here is utilized to qualitatively compare the comfort level between the two stiffness settings, whereas it does not represent the total contact force since the user's forearm was also partly supported by the lower support frame. The stiffness variation of the VSA and the RMS of sEMG signals in the VS trial are separately depicted in Fig. 15(c) and (d). As we can see, by real-time adjusting the stiffness of the VSA based on the subject's sEMG signals, the contact force curve measured in the VS trial exhibited greater flatness, and its peak amplitude was lower than that in the MS trial.

The average contact force for each subject is reported in Table III. Although their values varied slightly among subjects due to the minor shift of detection position on each individual, a general trend of lower contact force was seen in the VS trial, in which the value decreased by 47.2% (from 2.29 N to 1.21 N) on average compared with that in the MS trial. Therefore, the PVSED with sEMG-based real-time stiffness variation was capable of providing higher comfort to the user, demonstrated by the decreased contact force.

C. Safety Loop for the Proposed Bilateral Rehabilitation System

For a wearable rehabilitation device, the highest priority must be given to the user's safety. When performing robot-assisted rehabilitation, sudden involuntary muscle contractions (e.g., spasms) may cause undesired motions and generate excessive

Authorized licensed use limited to: Tianjin University of Technology. Downloaded on May 13,2021 at 11:53:56 UTC from IEEE Xplore. Restrictions apply.

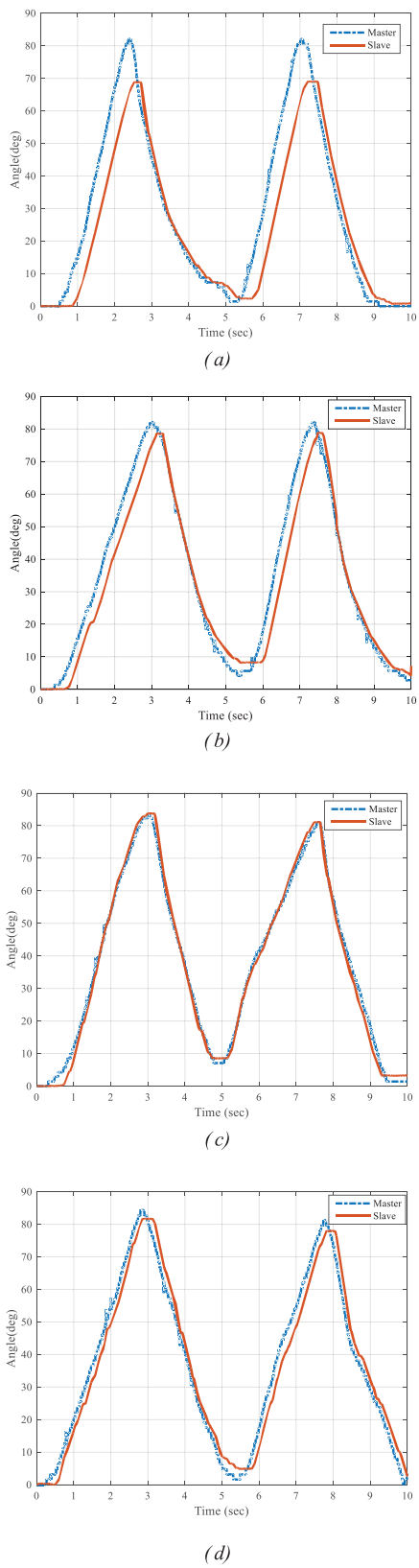

Fig. 13. Trajectories of the elbow joint in the bilateral rehabilitation task. (a) LS. (b) MS. (c) HS. (d) VS.

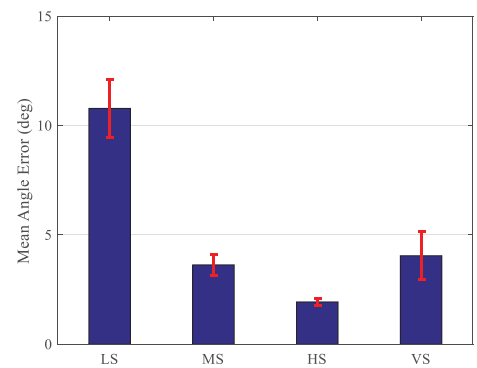

Fig. 14. Average tracking error of the ten subjects in different stiffness settings.

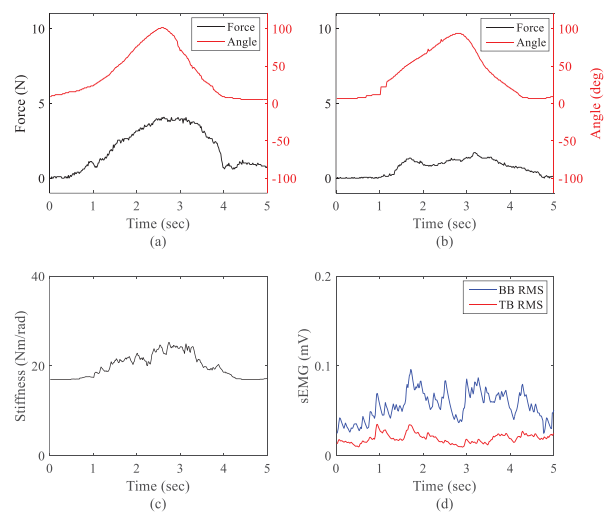

Fig. 15. Recorded experimental data in one cycle of elbow motion for Subject A. (a) Measured contact force and elbow angle in the MS trial. (b) Measured contact force and elbow angle in the VS trial. (c) Stiffness variation of the VSA in the VS trial. (d) The RMS of BB and TB in the VS trial.

TABLE III
CONTACT FORCE MEASUREMENT

Subject	Average force in the MS trial (N)	Average force in the VS trial (N)	Reduction rate
A	1.96	0.89	54.6%
B	2.01	1.24	38.3%
C	2.48	1.17	52.8%
D	1.75	1.03	41.1%
E	2.17	0.98	54.8%
F	2.76	1.29	53.3%
G	3.04	1.61	47.0%
H	1.85	0.97	47.6%
I	2.23	1.36	39.0%
J	2.64	1.58	40.2%
Average	2.29	1.21	47.2%

Authorized licensed use limited to: Tianjin University of Technology. Downloaded on May 13,2021 at 11:53:56 UTC from IEEE Xplore. Restrictions apply.

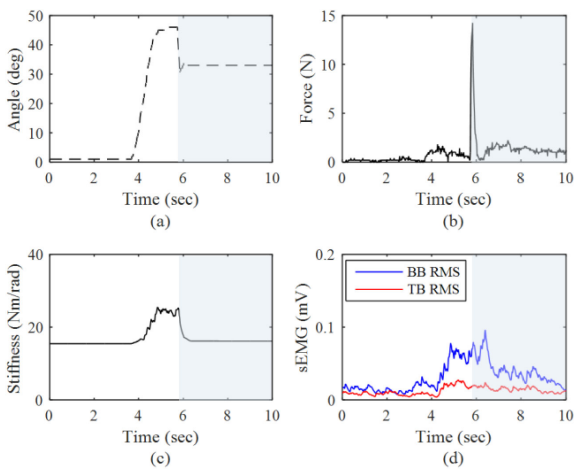

Fig. 16. Implementation of the safety loop. (a) Elbow angle on the slave side. (b) Measured contact force. (c) Stiffness variation of the VSA. (d) The RMS of BB and TB. The responses after triggering the safety loop are shown in the light-blue shaded area.

interaction forces between human and exoskeletal joints, which may pose a potential risk, even secondary damage to the patient. To address this issue, the proposed bilateral rehabilitation system implements a safety loop using the embedded force and angle sensors to monitor the potential risk. Once the measured force exceeds 12 N, or the robotic angular velocity is larger than 150°/s, the safety loop will be triggered to switch off the power motor immediately. Meanwhile, the sEMG-based joint stiffness control will fail to work, and the VSA motor will drive the pivot to return to its original position, where has the minimum stiffness.

To evaluate the effectiveness and response speed of the safety loop, a preliminary test was designed and conducted on a healthy subject. First, the subject's right upper limb was passively driven by the PVSED to perform robot-assisted bilateral elbow flexion. Then, commanded by the instructor, the subject suddenly exerted an opposite force on the mounted support frame against the movement trend, which mimics the typical symptoms of spasms. During this procedure, the subject's elbow trajectory on the slave side, interaction force with the upper support frame, the sEMG signals from the contralateral arm and the real-time stiffness of the VSA were simultaneously recorded, as shown in Fig. 16. It is evident that when the interaction force exceeded the threshold at 5.79 s (see Fig. 16(b)), the safety loop was automatically triggered and the actuation motor of the PVSED was switched off immediately (see Fig. 16(a)). Regardless of the sEMG signals variation (see Fig. 16(d)), the stiffness of the VSA was regulated to the lowest level to prevent uncomfortable or even painful interaction (see Fig. 16(c)). Note that after triggering the safety loop, the angular displacement on the slave side (from 46.1° to 33.7°) in Fig. 16(a) primarily resulted from the stiffness variation of the VSA, since a lower stiffness allowed an increasing angular deviation to avoid excessive interaction force. With the aid of the safety loop, the proposed bilateral rehabilitation system is capable of taking immediate measures to ensure the patient's safety even in case of emergency.

VI. Discussion

Robot-assisted bilateral training has been proven to be an effective method for patients with hemiparesis to promote the recovery process after stroke [51]. Various studies have focused on providing synchronized bilateral elbow movements by means of robotic systems. Song *et al.* designed a wearable exoskeleton device that makes use of an inertia sensor to implement synchronized human-robot elbow movements [52]. Although this method is meaningful and easy to be implemented, the human-robot interaction (HRI) is insufficient since the control loop cannot get any feedback from the patient. In order to enhance the HRI, Zhang *et al.* presented a coordinative motion-based bilateral rehabilitation system, which used a haptic device to provide tactile feedback to the operator [53]. However, the tactile feedback is only used to give hints about the tracking error rather than adjust the robotic assistance. Taking account of the close interaction with the patient, comfort is a major concern for wearable rehabilitation robots. For ensuring a comfortable HRI, different methods have been proposed to provide appropriate assistance to the patient. Lenzi *et al.* presented a proportional EMG-based control for a powered upper limb exoskeleton NEUROExos [54]. This method provides a rough estimation of the required torque assistance by proportionally scaling the patient's sEMG signals without specific calculation. Although it showed the effect on lowering the muscular effort, the patients might not be able to obtain assistance as needed for multiple rehabilitation tasks. In order to provide an assist-as-needed torque field, Chen *et al.* implemented an independent toque control on a cable-driven elbow exoskeleton CAREX [55]. The robotic torque is generated by two series elastic actuators (SEAs), which incorporate elastic elements to generate variable stiffness of the actuation system. Based on an encoder to measure the joint displacement angle thereby estimating the desired torque, the SEAs regulate the actuated stiffness to provide assistance as needed to the user. Nevertheless, this adjustment is passively depended on the measured encoder signals, whereas the patient's motion intention has not been actively explored.

In this paper, we present an sEMG-based stiffness control method that makes use of the individual's sEMG signals to achieve intention-guided stiffness adjustment of the PVSED. Firstly, an sEMG-driven musculoskeletal model was developed to characterize the properties of the human joint and subsequently validated in both isometric contraction (static force estimation - Fig. 9) and dynamic contraction (continuous torque estimation - Fig. 10). Based on this model, the proposed bilateral system implements an sEMG-based joint stiffness control to provide individual-specific and task-oriented stiffness variation. In the designed rehabilitation task with different training intensities, the subjects were capable of adjusting the stiffness of the VSA in real time by modulating their sEMG signals (sEMG-based stiffness variation - Fig. 11). Benefiting from this characteristic, the proposed bilateral rehabilitation system can present a fast adaptation to the patient's dynamic motions, thereby ensuring the tracking accuracy as well as the comfort during robot-assisted movement (system performance evaluation - Fig. 13-15 and Table III). Finally, we tested the response

Authorized licensed use limited to: Tianjin University of Technology. Downloaded on May 13,2021 at 11:53:56 UTC from IEEE Xplore. Restrictions apply.

of the safety loop in the proposed system by simulating an emergency, and the results showed it enabled fast switching of actuation to protect the user's safety (safety loop implementation - Fig. 16).

While these are significant advantages and promising prospects for home-based upper limb rehabilitation, some limitations of this study need to be noted and addressed in the near future. Firstly, it was noticed in Fig. 13 that a movement delay of nearly 0.5 s on the slave side occurs in each initial stage of the master-slave elbow position tracking, even in the case of high stiffness. This hysteresis is primarily caused by the backlash of cable-driven mechanism. Agrawal *et al.* suggested that the backlash is an intrinsic characteristic of cable transmission [56]. Although increasing the preload tension of the driven cables may have some effects on restraining this hysteresis, an adaptive backlash compensation control strategy is preferred to minimize this negative effect. Secondly, the proposed bilateral rehabilitation system only achieved passive rehabilitation training thus far. The real-time elbow position and stiffness trend on the contralateral arm are mirrored to the impaired arm by means of the exoskeleton. This strategy is meaningful in the initial stage of rehabilitation, in which the patient lost his/her motor ability on the affected side and has urgent demands on repetitive movement training to recover the impaired motor function. However, after the patient regained a partial control ability of the affected upper limb, an intensive rehabilitation therapy emphasizing on the active participation of patients is the preferred recommendation to facilitate the recovery process. The usage of sEMG signals from the affected side may be a promising approach to encourage active rehabilitation practice. Thirdly, the preliminary evaluation of the proposed rehabilitation system was only conducted on healthy subjects. Rehabilitation trials with stroke patients are expected to be involved in the near future for further evaluation.

VII. Conclusion

This paper presents a novel bilateral rehabilitation system that implements an sEMG-based real-time stiffness control to facilitate efficient and comfortable home-based upper limb rehabilitation. Since the stiffness of the human elbow joint varies during movement, an sEMG-driven musculoskeletal model that incorporates the muscle activation and muscular contraction dynamics was developed to describe the dynamic properties of the upper limb. Based on this model, the reference signals including the real-time elbow angle and stiffness profiles are provided to guide the operation of the exoskeleton device in order to achieve natural and comfortable human-robot coordinated movements. The proposed sEMG-based stiffness control enabled the robot to offer an individual-specific and task-oriented stiffness adjustment based on the patient's sEMG signals. Benefiting from this approach, the proposed rehabilitation system has the potential to present fast adaptation to the patient's dynamic motions a well as improving comfort during robot-assisted movement training.

Preliminary experiments were carried out to evaluate the feasibility of the proposed sEMG-based joint stiffness control and characterize the performance of the novel bilateral rehabilitation system. In the lifting trial with different load weights, the experimental results showed that the proposed sEMG-based joint stiffness control method allowed the subjects to real-time adjust the stiffness of the VSA by their sEMG signals to adapt to different task requirements. Furthermore, the subsequent bilateral rehabilitation task showed that with the aid of the sEMG-based real-time stiffness variation, the proposed bilateral rehabilitation system achieved promising results in both tracking accuracy and comfortability.

Future work will focus on using the sEMG signals from the affected side to encourage active practice. Attention will also be drawn to reduce the complexity of the calculation procedures.

References

[1] E. J. Benjamin, P. Muntner, and M. S. Bittencourt, "Heart disease and stroke statistics-2019 update: A report from the American Heart Association," *Circulation*, vol. 139, no. 10, 2019, Paper. e56-e528.

[2] S. Association, *State of the Nation: Stroke Statistics*, London, U. K.: Stroke Association, 2016.

[3] H. I. Krebs, "Twenty+ years of robotics for upper-extremity rehabilitation following a stroke," in *Rehabilitation Robotics*, Amsterdam, The Netherlands: Elsevier, 2018, pp. 175–192, doi: 10.1016/B978-0-12-811995-2.00013-8.

[4] G. Vanpee, G. Hermans, J. Segers, and R. Gosselink, "Assessment of limb muscle strength in critically ill patients: A systematic review," *Crit. Care Med.*, vol. 42, no. 3, pp. 701–711, 2014.

[5] A. Frisoli *et al.*, "Positive effects of robotic exoskeleton training of upper limb reaching movements after stroke," *J. Neuroeng. Rehabil.*, vol. 9, no. 1, p. 36, 2012, doi: 10.1186/1743-0003-9-36.

[6] M. Babaiasl, S. H. Mahdioun, P. Jaryani, and M. Yazdani, "A review of technological and clinical aspects of robot-aided rehabilitation of upper-extremity after stroke," *Disability Rehabil.: Assistive Technol.*, vol. 11, no. 4, pp. 263–280, 2016.

[7] J. M. Veerbeek, A. C. Langbroek-Amersfoort, E. E. van Wegen, C. G. Meskers, and G. Kwakkel, "Effects of robot-assisted therapy for the upper limb after stroke: A systematic review and meta-analysis," *Neurorehabil. Neural Repair*, vol. 31, no. 2, pp. 107–121, 2017.

[8] S. M. Waller and J. Whitall, "Bilateral arm training: Why and who benefits?," *NeuroRehabilitation*, vol. 23, no. 1, pp. 29–41, 2008.

[9] A. R. Luft *et al.*, "Repetitive bilateral arm training and motor cortex activation in chronic stroke: A randomized controlled trial," *JAMA*, vol. 292, no. 15, pp. 1853–1861, 2004.

[10] N. Vitiello *et al.*, "NEUROExos: A powered elbow exoskeleton for physical rehabilitation," *IEEE Trans. Robot.*, vol. 29, no. 1, pp. 220–235, Feb. 2013.

[11] X. Cui, W. Chen, X. Jin, and S. K. Agrawal, "Design of a 7-DOF cable-driven arm exoskeleton (CAREX-7) and a controller for dexterous motion training or assistance," *IEEE/ASME Trans. Mechatronics*, vol. 22, no. 1, pp. 161–172, Feb. 2017.

[12] P. M. Chen, P. W. Kwong, C. K. Lai, and S. S M Ng, "Comparison of bilateral and unilateral upper limb training in people with stroke: A systematic review and meta-analysis," *PLoS One*, vol. 14, 2019, Paper e0216357.

[13] P. H. Chang and S. H. Kang, "Stochastic estimation of human arm impedance under nonlinear friction in robot joints: A model study," *J. Neurosci. Methods*, vol. 189, no. 1, pp. 97–112, 2010.

[14] K. P. Tee, D. W. Franklin, M. Kawato, T. E. Milner, and E. Burdet, "Concurrent adaptation of force and impedance in the redundant muscle system," *Biol. Cybern.*, vol. 102, no. 1, pp. 31–44, 2010.

[15] M. Simkins, N. Byl, H. Kim, G. Abrams, and J. Rosen, "Upper limb bilateral symmetric training with robotic assistance and clinical outcomes for stroke: A pilot study," *Int. J. Intell. Comput. Cybern.*, vol. 9, no. 1, pp. 83–104, 2016.

[16] Y.-W. Hsieh *et al.*, "Bilateral robotic priming before task-oriented approach in subacute stroke rehabilitation: A pilot randomized controlled trial," *Clin. Rehabil.*, vol. 31, no. 2, pp. 225–233, 2017.

[17] S. A. Migliore, E. A. Brown, and S. P. DeWeerth, "Biologically inspired joint stiffness control," in *Proc. IEEE Int. Conf. Robot. Automat.* , 2005, pp. 4508–4513.

[18] M. Pang, S. Guo, and S. Zhang, "Prediction of interaction force using EMG for characteristic evaluation of touch and push motions," in *Proc. IEEE/RSJ Int. Conf. Intell. Robots Syst.*, 2015, pp. 2099–2104.

Authorized licensed use limited to: Tianjin University of Technology. Downloaded on May 13,2021 at 11:53:56 UTC from IEEE Xplore. Restrictions apply.

[19] D. Toledo-Pérez, M. Martínez-Prado, R. Gómez-Loenzo, W. Paredes-García, and J. Rodríguez-Reséndiz, "A study of movement classification of the lower limb based on up to 4-EMG channels," *Electronics*, vol. 8, 2019, doi: 10.3390/electronics8030259.

[20] D. C. Toledo-Perez, J. Rodriguez-Resendiz, and R. A. Gomez-Loenzo, "A study of computing zero crossing methods and an improved proposal for EMG signals," *IEEE Access*, vol. 8, pp. 8783–8790, 2020.

[21] Z. Li, B. Wang, F. Sun, C. Yang, Q. Xie, and W. Zhang, "sEMG-based joint force control for an upper-limb power-assist exoskeleton robot," *IEEE J. Biomed. Health Inform.*, vol. 18, no. 3, pp. 1043–1050, May 2014.

[22] F. Xiao, "Proportional myoelectric and compensating control of a cable-conduit mechanism-driven upper limb exoskeleton," *ISA Trans.*, vol. 89, pp. 245–255, 2019.

[23] J. S. Knutson, M. Y. Harley, T. Z. Hisel, N. S. Makowski, and J. Chae, "Contralaterally controlled functional electrical stimulation for recovery of elbow extension and hand opening after stroke: A pilot case series study," *Amer. J. Phys. Med. Rehabil./Assoc. Academic Physiatrists*, vol. 93, no. 6, pp. 528–539, 2014.

[24] Y. Liu, S. Guo, H. Hirata, H. Ishihara, and T. Tamiya, "Development of a powered variable-stiffness exoskeleton device for elbow rehabilitation," *Biomed. Microdevices*, vol. 20, 2018, doi: 10.1007/s10544-018-0312-6.

[25] T. Nef, M. Guidali, and R. Riener, "ARMin III–arm therapy exoskeleton with an ergonomic shoulder actuation," *Appl. Bionics Biomechanics*, vol. 6, no. 2, pp. 127–142, 2009.

[26] S. S. Groothuis, G. Rusticelli, A. Zucchelli, S. Stramigioli, and R. Carloni, "The variable stiffness actuator vsaut-ii: Mechanical design, modeling, and identification," *IEEE/ASME Trans. Mechatronics*, vol. 19, no. 2, pp. 589–597, Apr. 2014.

[27] C. Fang, A. Ajoudani, A. Bicchi, and N. G. Tsagarakis, "Online model based estimation of complete joint stiffness of human arm," *IEEE Robot. Automat. Lett.*, vol. 3, no. 1, pp. 84–91, Jan. 2018.

[28] J. Potvin and S. Brown, "Less is more: High pass filtering, to remove up to 99% of the surface EMG signal power, improves EMG-based biceps brachii muscle force estimates," *J. Electromyogr. Kinesiol.*, vol. 14, no. 3, pp. 389–399, 2004.

[29] P. Konrad, "The abc of emg," *A Practical Introduction to Kinesiological Electromyography*, vol. 1, pp. 30–35, 2005.

[30] D. G. Lloyd and T. F. Besier, "An EMG-driven musculoskeletal model to estimate muscle forces and knee joint moments in vivo," *J. Biomechanics*, vol. 36, no. 6, pp. 765–776, 2003.

[31] K. D. Nguyen, N. Sharma, and M. Venkadesan, "Active viscoelasticity of sarcomeres," *Front. Robot. AI*, vol. 5, pp. 1–9, 2018, doi: 10.3389/frobt.2018.00069.

[32] P. Bujalski, J. Martins, and L. Stirling, "A Monte Carlo analysis of muscle force estimation sensitivity to muscle-tendon properties using a Hill-based muscle model," *J. Biomechanics*, vol. 79, pp. 67–77, 2018, doi: 10.1016/j.jbiomech.2018.07.045.

[33] F. Romero and F. Alonso, "A comparison among different Hill-type contraction dynamics formulations for muscle force estimation," *Mech. Sci.*, vol. 7, no. 1, pp. 19–29, 2016.

[34] Q. Ding, X. Zhao, A. Xiong, and J. Han, "A novel motion estimate method of human joint with EMG-driven model," in *Proc. IEEE Int. Conf. Bioinf. Biomed. Eng.*, 2011, pp. 1–5.

[35] K. R. Holzbaur, W. M. Murray, and S. L. Delp, "A model of the upper extremity for simulating musculoskeletal surgery and analyzing neuromuscular control," *Ann. Biomed. Eng.*, vol. 33, no. 6, pp. 829–840, 2005.

[36] J. Han, Q. Ding, A. Xiong, and X. Zhao, "A state-space EMG model for the estimation of continuous joint movements," *IEEE Trans. Ind. Electron.*, vol. 62, no. 7, pp. 4267–4275, Jul. 2015.

[37] T. S. Buchanan, D. G. Lloyd, K. Manal, and T. F. Besier, "Neuromusculoskeletal modeling: Estimation of muscle forces and joint moments and movements from measurements of neural command," *J. Appl. Biomechanics*, vol. 20, no. 4, pp. 367–395, 2004.

[38] Z. Li, Z. Huang, W. He, and C.-Y. Su, "Adaptive impedance control for an upper limb robotic exoskeleton using biological signals," *IEEE Trans. Ind. Electron.*, vol. 64, no. 2, pp. 1664–1674, Feb. 2017.

[39] C. Fleischer and G. Hommel, "A human–exoskeleton interface utilizing electromyography," *IEEE Trans. Robot.*, vol. 24, no. 4, pp. 872–882, Aug. 2008.

[40] K. An, K. Takahashi, T. Harrigan, and E. Chao, "Determination of muscle orientations and moment arms," *J. Biomech. Eng.*, vol. 106, pp. 280–282, Aug. 1984.

[41] N. Karavas, A. Ajoudani, N. Tsagarakis, J. Saglia, A. Bicchi, and D. Caldwell, "Tele-impedance based assistive control for a compliant knee exoskeleton," *Robot. Auton. Syst.*, vol. 73, pp. 78–90, 2015.

[42] T. D'Alessio and S. Conforto, "Extraction of the envelope from surface EMG signals," *IEEE Eng. Med. Biol. Mag.*, vol. 20, no. 6, pp. 55–61, Nov./Dec. 2001.

[43] F. Günzkofer, F. Engstler, H. Bubb, and K. Bengler, "Isometric elbow flexion and extension joint torque measurements considering biomechanical aspects," in *Proc. 1st Int. Symp. Digital Hum. Model.*, 2011, pp. 14–15.

[44] A. Ajoudani, N. G. Tsagarakis, and A. Bicchi, "Tele-impedance: Teleoperation with impedance regulation using a body-machine interface," *Int. J. Robot. Res.*, vol. 31, no. 13, pp. 1642–1656, 2012.

[45] NUMBERS - Curiosities, theory and uses. 2014. [Online]. Available: http://villemin.gerard.free.fr/Biologie/CorpsMS.htm

[46] U. R. Acharya *et al.*, "Characterization of focal EEG signals: A review," *Future Gener. Comput. Syst.*, vol. 91, pp. 290–299, Feb. 2019.

[47] F. A. Elhaj, N. Salim, A. R. Harris, T. T. Swee, and T. Ahmed, "Arrhythmia recognition and classification using combined linear and nonlinear features of ECG signals," *Comput. Methods Programs Biomed.*, vol. 127, pp. 53–63, 2016.

[48] K. Kiguchi and Y. Hayashi, "An EMG-based control for an upper-limb power-assist exoskeleton robot," *IEEE Trans. Syst. Man Cybern. Part B Cybern.*, vol. 42, no. 4, pp. 1064–1071, Aug. 2012.

[49] D. C. Toledo-Pérez, J. Rodríguez-Reséndiz, R. A. Gómez-Loenzo, and J. C. Jauregui-Correa, "Support vector machine-based EMG signal classification techniques: A review," *Appl. Sci.*, vol. 9, 2019, Art. no. 4402.

[50] T. Lenzi, N. Vitiello, S. M. M. De Rossi, S. Roccella, F. Vecchi, and M. C. Carrozza, "NEUROExos: A variable impedance powered elbow exoskeleton," in *Proc. IEEE Int. Conf. Robot. Automat.*, 2011, pp. 1419–1426.

[51] J. H. Cauraugh, N. Lodha, S. K. Naik, and J. J. Summers, "Bilateral movement training and stroke motor recovery progress: A structured review and meta-analysis," *Hum. Movement Sci.*, vol. 29, no. 5, pp. 853–870, 2010.

[52] Z. Song and S. Guo, "Design process of exoskeleton rehabilitation device and implementation of bilateral upper limb motor movement," *J. Med. Biol. Eng.*, vol. 32, no. 5, pp. 323–330, 2012.

[53] S. Zhang, Q. Fu, S. Guo, and Y. Fu, "Coordinative motion-based bilateral rehabilitation training system with exoskeleton and haptic devices for biomedical application," *Micromachines*, vol. 10, p. 8, 2019.

[54] T. Lenzi, S. M. M. De Rossi, N. Vitiello, and M. C. Carrozza, "Intention-based EMG control for powered exoskeletons," *IEEE Trans. Biomed. Eng.*, vol. 59, no. 8, pp. 2180–2190, Aug. 2012.

[55] T. Chen, R. Casas, and P. S. Lum, "An elbow exoskeleton for upper limb rehabilitation with series elastic actuator and cable-driven differential," *IEEE Trans. Robot.*, vol. 35, no. 6, pp. 1464–1474, Dec. 2019.

[56] V. Agrawal, W. J. Peine, B. Yao, and S. Choi, "Control of cable actuated devices using smooth backlash inverse," in *Proc. IEEE Int. Conf. Robot. Automat.*, 2010, pp. 1074–1079.

Authorized licensed use limited to: Tianjin University of Technology. Downloaded on May 13,2021 at 11:53:56 UTC from IEEE Xplore. Restrictions apply.